

Observation of electron states of small period artificial graphene in nano-patterned GaAs quantum wells

Sheng Wang, Diego Scarabelli, Yuliya Y. Kuznetsova, Shalom J. Wind, Aron Pinczuk, Vittorio Pellegrini, Michael J. Manfra, Geoff C. Gardner, Loren N. Pfeiffer, and Ken W. West

Citation: *Applied Physics Letters* **109**, 113101 (2016); doi: 10.1063/1.4962461

View online: <http://dx.doi.org/10.1063/1.4962461>

View Table of Contents: <http://scitation.aip.org/content/aip/journal/apl/109/11?ver=pdfcov>

Published by the AIP Publishing

Articles you may be interested in

[Fabrication of artificial graphene in a GaAs quantum heterostructure](#)

J. Vac. Sci. Technol. B **33**, 06FG03 (2015); 10.1116/1.4932672

[Spin and charge effects due to positively charged acceptors in GaAs/AlGaAs quantum wells](#)

Low Temp. Phys. **41**, 90 (2015); 10.1063/1.4913583

[Intersubband transition energy and linewidth modified by a submonolayer AlAs insertion into GaAs quantum wells](#)

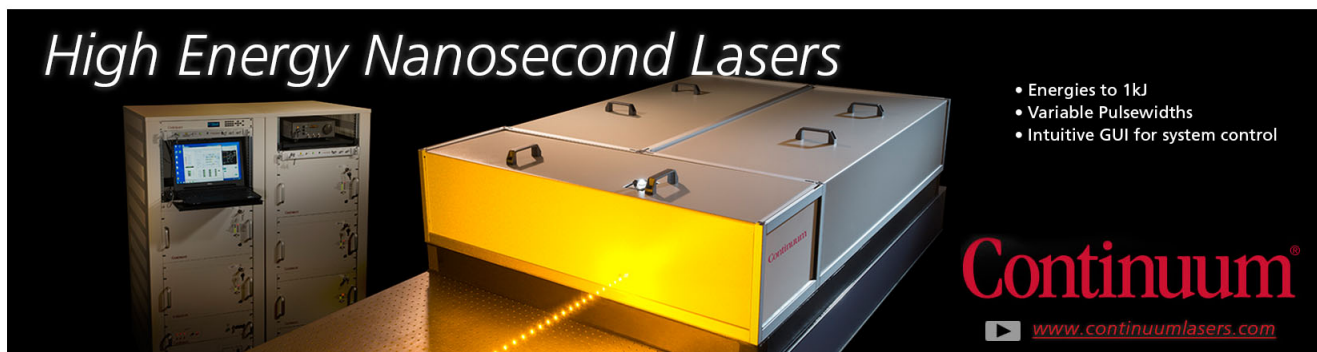
J. Appl. Phys. **109**, 043506 (2011); 10.1063/1.3549126

[Effects of interface roughness and phonon scattering on intersubband absorption linewidth in a GaAs quantum well](#)

Appl. Phys. Lett. **78**, 3448 (2001); 10.1063/1.1376154

[Optical properties of InAlGaAs quantum wells: Influence of segregation and band bowing](#)

J. Appl. Phys. **86**, 2584 (1999); 10.1063/1.371096

The advertisement features a large, industrial-grade laser system with a prominent yellow light output. To the left, a control rack with multiple modules and a monitor is visible. The background is dark, making the laser and its components stand out. The text 'High Energy Nanosecond Lasers' is written in a large, white, serif font at the top left. On the right, a list of features is provided in white text. The Continuum logo, in a stylized red font, is positioned at the bottom right, with the website address below it.

High Energy Nanosecond Lasers

- Energies to 1kJ
- Variable Pulsewidths
- Intuitive GUI for system control

Continuum[®]

www.continuumlasers.com

Observation of electron states of small period artificial graphene in nano-patterned GaAs quantum wells

Sheng Wang,^{1,a)} Diego Scarabelli,¹ Yuliya Y. Kuznetsova,² Shalom J. Wind,¹ Aron Pinczuk,^{1,2,b)} Vittorio Pellegrini,^{3,4} Michael J. Manfra,^{5,6,7} Geoff C. Gardner,⁶ Loren N. Pfeiffer,⁸ and Ken W. West⁸

¹*Department of Applied Physics and Applied Mathematics, Columbia University, New York, New York 10027, USA*

²*Department of Physics, Columbia University, New York, New York 10027, USA*

³*Graphene Labs, Istituto Italiano di Tecnologia, Via Morego 30, I-16163 Genova, Italy*

⁴*NEST, Istituto Nanoscienze-CNR and Scuola Normale Superiore, I-56126 Pisa, Italy*

⁵*Department of Physics and Astronomy, Birck Nanotechnology Center, Purdue University, West Lafayette, Indiana 47907, USA*

⁶*School of Materials Engineering, Birck Nanotechnology Center, Purdue University, West Lafayette, Indiana 47907, USA*

⁷*School of Electrical and Computer Engineering, Birck Nanotechnology Center, Purdue University, West Lafayette, Indiana 47907, USA*

⁸*Department of Electrical Engineering, Princeton University, Princeton, New Jersey 08544, USA*

(Received 24 June 2016; accepted 26 August 2016; published online 12 September 2016)

Engineered honeycomb lattices, called artificial graphene (AG), are tunable platforms for the study of novel electronic states related to Dirac physics. In this work, we report the achievement of electronic bands of the honeycomb topology with the period as low as 40 nm on the nano-patterned modulation-doped AlGaAs/GaAs quantum wells. Resonant inelastic light scattering spectra reveal peaks which are interpreted as combined electronic transitions between subbands of the quantum well confinement with a change in the AG band index. Spectra lineshapes are explained by joint density of states obtained from the calculated AG electron band structures. These results provide a basis for further advancements in AG physics. *Published by AIP Publishing.*
[\[http://dx.doi.org/10.1063/1.4962461\]](http://dx.doi.org/10.1063/1.4962461)

Graphene consists of a single layer of carbon atoms arranged in a honeycomb lattice. Charge carriers in graphene have a linear energy-momentum dispersion that has led them to be characterized as massless Dirac fermions (MDFs).^{1–3} The MDFs that result from the symmetry of the lattice should be observable in other systems with a similar topology. Unlike natural graphene, an artificial honeycomb lattice offers tunable parameters such as intersite spacing and coupling that allow for the exploration of the fascinating physics of the electron states associated with the honeycomb topology further than possible in natural graphene.⁴ So far, Dirac physics in artificial graphene (AG) potentials have been achieved in molecular⁵ and optical lattices.⁶ Particularly promising would be the realization of Dirac physics in semiconductor systems, where the nanofabrication methods offer a great design flexibility and easier integration with the optoelectronic components.

Nano-patterned semiconductor quantum well (QW) structures hosting an ultrahigh-mobility two-dimensional electron gas (2DEG), called lateral superlattices, were intensively studied in the late 1980s and 1990s.^{7–11} Creation of superlattices with observable minibands requires extremely low disorder QW, high lattice uniformity, and especially small lattice constant. These requirements impose substantial challenges to the fabrication technologies. Evaluations of electron bands of AG lattices in the nano-patterned semiconductor QWs^{12–15} show

that the AG lattice constants required to see that the well-defined AG bands are significantly smaller¹⁶ than those fabricated in this type of system to date.^{13,17–19}

We recently demonstrated AG lattices in the nano-patterned GaAs QWs with lattice constants as small as 40 nm,²⁰ which is the current state of the art. We have used these to explore the formation of AG electron bands in small period honeycomb lattices. In this paper, we present evidence of AG electron band structures in such artificial lattices. Evidence of well-defined AG electron bands is found in the resonant inelastic light scattering (RILS) spectra of inter-subband transitions. The spectra reveal peaks which are interpreted as combined electronic transitions between the subbands of the quantum well confinement with a change in the AG band index. Those transitions are well explained by a calculation of the joint density of states (JDOS) in a fashion that reflects the underlying honeycomb lattice topology.

The formation of AG bands in the nano-patterned semiconductor systems creates tunable platforms for the study of AG physics. Dirac cones are expected to be well-developed within the parameter space of our lattices, as seen in our calculations.

Figure 1 describes the method for the realization of AG lattices in a GaAs QW. The fabricated AG lattices are superimposed on a two-dimensional electron gas confined within a 25 nm-wide one-side modulation-doped GaAs/Al_{0.1}Ga_{0.9}As QW (Fig. 1(a)). The QW is positioned 110 nm below the surface and 30 nm below the Si δ -doping layer. The as-grown electron density is $1.8 \times 10^{11} \text{ cm}^{-2}$, with the low-temperature

^{a)}Electronic mail: sw2677@columbia.edu

^{b)}Electronic mail: aron@phys.columbia.edu

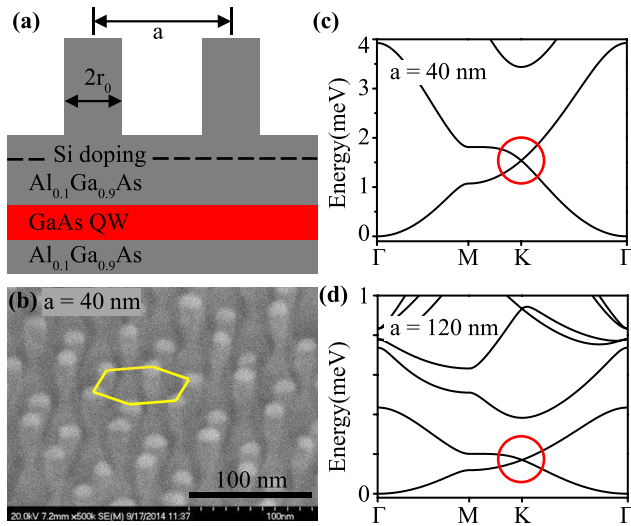


FIG. 1. Principle of realization of artificial graphene. (a) Cross-section schematic of the nano-patterned QW sample. (b) SEM image of an AG pattern with $a = 40$ nm. A hexagon is drawn for eye guidance. The radius of the potential used in the calculation, r , is smaller than the physical radius of pillars, r_0 , indicated in (a). (c) and (d) Calculated AG bands for different periods (c) $a = 40$ nm, $r = 11$ nm, $V_0 = -6.0$ meV and (d) $a = 120$ nm, $r = 34$ nm, $V_0 = -0.67$ meV. The Dirac cones at K and K' points are indicated by circles. For smaller period, the energy range of the linear dispersion around Dirac points is larger.

(~ 4 K) mobility of 3.2×10^6 cm²/(V s). A high-resolution electron beam lithography was used to create $200 \times 200 \mu\text{m}^2$ honeycomb arrays of metallic nano-disks, which serve as masks for etching. Inductively coupled plasma reactive-ion etching (ICP-RIE) was used to etch the samples to a depth of around 70 nm. Details of the fabrication procedure and optimization can be found in Ref. 20. The resulting pillars are arranged in a honeycomb lattice as shown in Fig. 1(b). The pillars act as attractive potentials V_0 for electrons in the GaAs QW. Sufficiently small feature size is necessary because the energy scale of the band structures is proportional to $1/a^2$. Figs. 1(c) and 1(d) show the calculated AG band structures for two different lattice periods, where the energy scale increases one order of magnitude when the lattice constant decreases from $a = 120$ nm to $a = 40$ nm. The potential used in this comparison is different for different lattice constants a , because the suitable potential required for the formation of well-developed Dirac cones scales as $1/a^2$.¹³ The band structure calculation in Figs. 1(c) and 1(d) was performed using a simplified muffin-tin potential similar to Ref. 13.

The samples were mounted in an optical cryostat operated at temperatures in the range of 4–5 K. The RILS measurements were performed in a back-scattering configuration, with the incident laser beam almost perpendicular (within 6°) to the sample. The emission of a tunable Ti:sapphire laser was focused onto the AG patterns to a spot of around $100 \mu\text{m}$ diameter with a typical power around 1 mW. The light scattered from the sample was directed through a double grating spectrometer and collected using a liquid nitrogen cooled CCD. Two polarization configurations were used. In cross configuration, the polarization of the scattered light is perpendicular to that of the incident light, while in parallel configuration the polarization direction is the same. We present results from two AG patterns with $a = 40$ nm and $a = 50$ nm.

Intersubband excitations observed in the RILS spectra offer a powerful method for probing the electron states produced by the AG lattice. Intersubband excitations deriving from the changes in the confinement in the QW are illustrated in the [supplementary material](#) (Fig. S1) for the as-grown sample. Collective modes have well-defined polarization selection rules.²¹ The single particle excitations at energy 21.8 meV (denoted by E_{01}^0) are independent of the polarization configuration.

The RILS spectra of intersubband excitations of the AG pattern with $a = 40$ nm, shown in Figs. 2(a) and 2(b), display a strong peak at 20.9 meV, denoted by E_{01} , accompanied by several weaker satellite peaks. The strong peak E_{01} is present in both polarizations and thus is interpreted as the single particle transition between the first two subbands of the QW confinement. It is red-shifted from E_{01}^0 due to a decrease in the 2DEG electron density after etching. The satellite peaks, *only present in the etched AG sample*, are interpreted in terms of combined transitions between subbands of QW confinement and electron states created by the periodic potential of the AG lattice, as schematically shown in Fig. 2(c). In these combined transitions, the change in the AG band index provides insight into physics associated with honeycomb topology.

In a simplified description, the RILS spectra in Figs. 2(a) and 2(b) are interpreted as proportional to the JDOS (see [supplementary material](#)) for combined intersubband transitions with the AG band index change, such as those shown in Fig. 2(c). The JDOS calculation (Fig. 3) includes different possible transitions in the energy range close to E_{01} and consists of both red-shifted and blue-shifted transitions. The JDOS is broadened by a Gaussian function with full width at half maximum (FWHM) of 0.2 meV.²² The calculated JDOS is based on the band structures shown in Fig. 2(c) and does not take into account the energy dependence of the RILS matrix element. The parameters in the calculation r , V_0 , and the Fermi energy, E_F , are first estimated from the experiments and then adjusted for the best fit of JDOS (see [supplementary material](#)). The uncertainties of the parameters for the best fit are: 0.4 nm for r , 0.2 meV for V_0 , and 0.1 meV for E_F . The radius of the potential used in modeling, r , is smaller than the physical radius of the pillars, r_0 , indicated in Fig. 1(a). Nevertheless, this simplified model provides a rather good interpretation of the satellite peaks.

To identify the energies of the satellite peaks E_R^1 , E_B^1 , and E_B^2 , we fit the spectra with multiple Lorentzian peaks. The results of the fit are shown in Fig. 3. The calculated JDOS has the maxima at energies that overlap with those of the satellite peaks. The strong peak of JDOS at E_{01} (lowest panel in Fig. 3) arises from transitions between the subbands with the same AG band index (such as transitions from c_{00} to c_{10} and from c_{01} to c_{11} in Fig. 2(c)), which involves parallel bands with a high JDOS. The red-shifted satellites E_R^1 and E_R^2 arise from transitions between c_{01} and c_{10} , while the blue-shifted satellites E_B^1 and E_B^2 from transitions between c_{01} and c_{12} . The shaded area E_R^2 of the JDOS in Fig. 3 overlaps the RILS signal seen at lower energies in the top spectrum of Fig. 2(a).

Results from the pattern with $a = 50$ nm are shown in Fig. 4. The red-shifted peak $E_R^{1,2}$ is resolved at lower incident

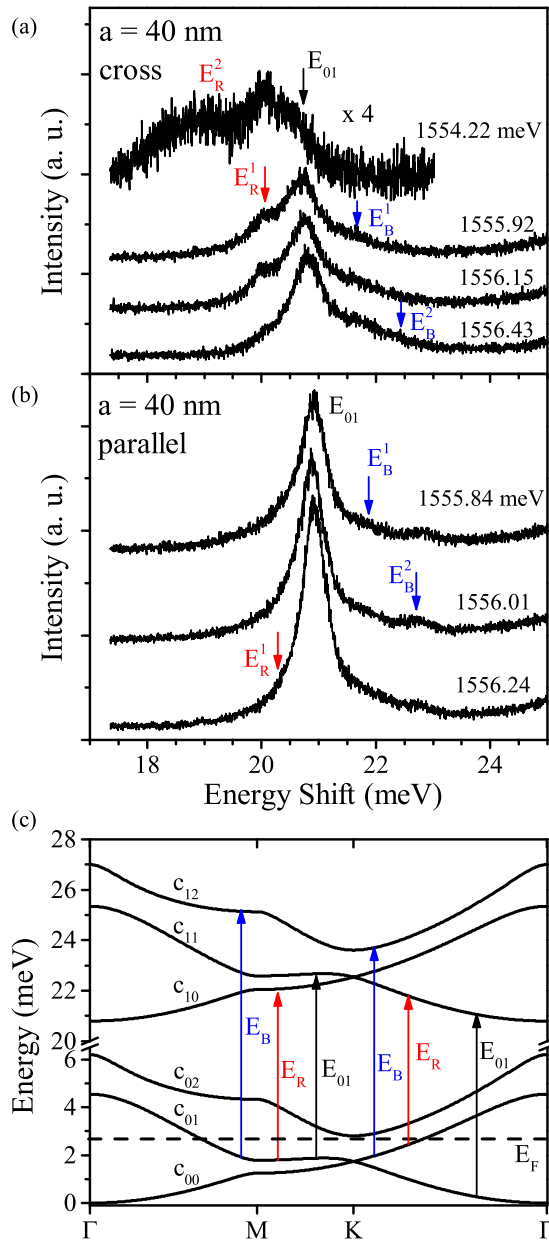


FIG. 2. RILS spectra of intersubband transitions involving AG bands. (a) Cross and (b) parallel polarization configurations for RILS spectra from the $a = 40$ nm pattern, the incident photon energies are indicated. The peaks are interpreted as transitions between subbands indicated in (c), the band structure calculated with parameters $a = 40$ nm, $r = 8.0$ nm, $V_0 = -6.1$ meV, and Fermi energy $E_F = 2.7$ meV. The vertical lines indicate transitions between subbands. The combined intersubband transitions with the change of subband and AG band are indicated in blue and red.

photon energy, while the blue-shifted peak $E_B^{1,2}$ is resolved at higher photon energy. The smaller energy scale here, due to the larger lattice constant, results in the more narrowly spaced features in the JDOS and single broader RILS satellite peaks $E_R^{1,2}$ and $E_B^{1,2}$ rather than separate peaks seen for the $a = 40$ nm pattern (Fig. 3). The results clearly demonstrate the impact of the lattice constant on the AG band structures.

Intersubband excitations from near the Dirac point are currently not resolved due to their overlap with the strong main peak E_{01} of the RILS spectra. We estimate the linear dispersion range of the AG band structures to be about

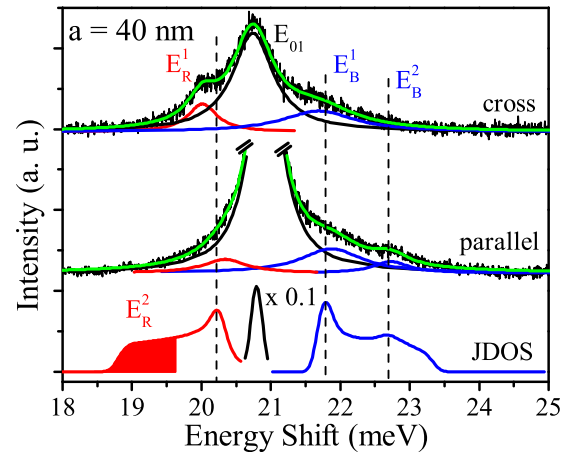


FIG. 3. Interpretation of RILS spectra in Fig. 2 as combined intersubband transitions for the $a = 40$ nm patterns. The calculated JDOS (bottom curves) is for the transitions indicated in Fig. 2(c). The central peak, shown in black, is rescaled for clarity. Combined intersubband transitions are shown in blue and red. The shaded area E_R^2 overlaps the RILS signal seen at lower energies in the top spectrum of Fig. 2(a). The peak positions in the RILS spectra (top curves) agree with the peaks observed in the JDOS. The parameters used for the calculation of JDOS are $a = 40$ nm, $r = 8.0$ nm, $V_0 = -6.1$ meV, and $E_F = 2.7$ meV.

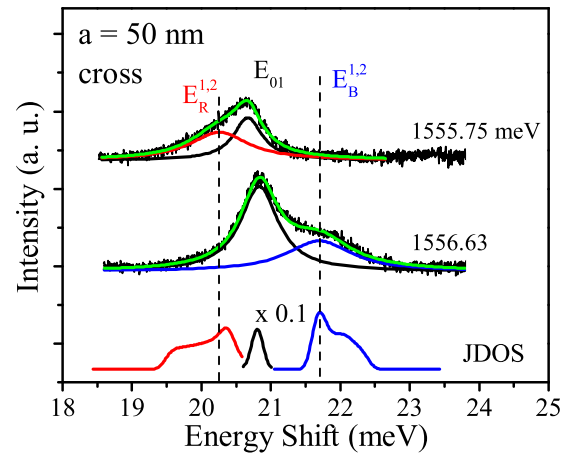


FIG. 4. RILS spectra of intersubband transitions for the $a = 50$ nm pattern, the incident photon energies are indicated. The combined intersubband transitions are shown in blue and red. The calculated JDOS is shown in the bottom panel. The blue and red curves in the JDOS have the maxima at energies that overlap the positions of the measured combined intersubband transitions. The parameters used for the calculation of JDOS are $a = 50$ nm, $r = 8.5$ nm, $V_0 = -6.4$ meV, and $E_F = 1.7$ meV.

0.5 meV for parameters used for the $a = 40$ nm pattern (Fig. 2(c)), large enough to be observed in the future using optical spectroscopy. The Fermi energy of AG lattices could additionally be controlled by gating, to provide access to transitions involving Dirac cones of the band structures.

In conclusion, we have found evidence of well-formed AG bands in a modulation-doped AlGaAs/GaAs QW patterned with small period honeycomb lattices. The RILS spectra reveal combined transitions with a simultaneous change of the AG band index and subband index that manifest as satellite peaks. This interpretation is well supported by the calculation of the JDOS. The fitted AG electron energy band structures suggest the presence of well-developed Dirac cones which future experiments should be able to access.

When the Fermi level is placed around the Dirac cone in the presence of a magnetic field, a \sqrt{B} dispersion^{23–25} of inter-Landau level transitions can provide further evidence of Dirac fermions. The realization of the AG lattices in a nano-fabricated high-mobility semiconductor system offers the advantage of tunability through the methods suitable for device scalability and integration. The implementation of such an AG lattice in materials with strong spin-orbit coupling should enable the exploration of topological insulating states with great tunability.^{26,27}

See [supplementary material](#) for intersubband excitations of the as-grown sample, definition of JDOS, and estimation of parameters for modeling.

The major activities in this project, including processing and characterization of AG lattices at Columbia University, were supported by Grant DE-SC0010695 funded by the U.S. Department of Energy Office of Science, Division of Materials Sciences and Engineering. Fabrication and processing at Columbia were performed in the CEPSCR Cleanroom under the auspices of the Columbia Nanoscience Initiative. Additional processing was carried out at the PRISM Micro/Nano Fabrication Laboratory at Princeton University. The authors thank George P. Watson for technical assistance with the ICP-RIE etching performed there. The growth of GaAs/AlGaAs QWs at Purdue University was supported by Grant DE-SC0006671 funded by the U.S. Department of Energy Office of Science, Division of Materials Sciences and Engineering. The growth of GaAs/AlGaAs QWs at Princeton University was supported by the Gordon and Betty Moore Foundation under Award GMBF-2719 and by the National Science Foundation, Division of Materials Research, under Award DMR-0819860. V.P. acknowledges the European Graphene Flagship (Contract No. CNECT-ICT-604391) for the financial support and the Italian Ministry of Research (MIUR) through the program “Progetti Premiali 2012”—Project “ABNANOTECH.” The authors are grateful to Antonio Levy and Fu Qiao at Columbia University for insightful discussions.

¹K. S. Novoselov, A. K. Geim, S. V. Morozov, D. Jiang, M. I. Katsnelson, I. V. Grigorieva, S. V. Dubonos, and A. A. Firsov, *Nature* **438**, 197 (2005).

- ²Y. B. Zhang, Y. W. Tan, H. L. Stormer, and P. Kim, *Nature* **438**, 201 (2005).
- ³A. H. Castro Neto, F. Guinea, N. M. R. Peres, K. S. Novoselov, and A. K. Geim, *Rev. Mod. Phys.* **81**, 109 (2009).
- ⁴M. Polini, F. Guinea, M. Lewenstein, H. C. Manoharan, and V. Pellegrini, *Nat. Nanotechnol.* **8**, 625 (2013).
- ⁵K. K. Gomes, W. Mar, W. Ko, F. Guinea, and H. C. Manoharan, *Nature* **483**, 306 (2012).
- ⁶L. Tarruell, D. Greif, T. Uehlinger, G. Jotzu, and T. Esslinger, *Nature* **483**, 302 (2012).
- ⁷G. Bernstein and D. K. Ferry, *J. Vac. Sci. Technol. B* **5**, 964 (1987).
- ⁸D. Weiss, K. v. Klitzing, K. Ploog, and G. Weimann, *Europhys. Lett.* **8**, 179 (1989).
- ⁹J. S. Weiner, G. Danan, A. Pinczuk, J. Valladares, L. N. Pfeiffer, and K. West, *Phys. Rev. Lett.* **63**, 1641 (1989).
- ¹⁰T. Egeler, G. Abstreiter, G. Weimann, T. Demel, D. Heitmann, P. Grambow, and W. Schlapp, *Phys. Rev. Lett.* **65**, 1804 (1990).
- ¹¹D. Heitmann and J. P. Kotthaus, *Phys. Today* **46**(6), 56 (1993).
- ¹²C. H. Park and S. G. Louie, *Nano Lett.* **9**, 1793 (2009).
- ¹³M. Gibertini, A. Singha, V. Pellegrini, M. Polini, G. Vignale, A. Pinczuk, L. N. Pfeiffer, and K. W. West, *Phys. Rev. B* **79**, 241406 (2009).
- ¹⁴E. Rasanen, C. A. Rozzi, S. Pittalis, and G. Vignale, *Phys. Rev. Lett.* **108**, 246803 (2012).
- ¹⁵I. Kylanpaa, M. Aichinger, S. Janecek, and E. Rasanen, *J. Phys. Condens. Matter* **27**, 425501 (2015).
- ¹⁶In order to have a Dirac cone with linear dispersion range of about 0.5 meV, the distance between two pillars in honeycomb lattice need to be about 40 nm.
- ¹⁷G. De Simoni, A. Singha, M. Gibertini, B. Karmakar, M. Polini, V. Piazza, L. N. Pfeiffer, K. W. West, F. Beltram, and V. Pellegrini, *Appl. Phys. Lett.* **97**, 132113 (2010).
- ¹⁸A. Singha, M. Gibertini, B. Karmakar, S. Yuan, M. Polini, G. Vignale, M. I. Katsnelson, A. Pinczuk, L. N. Pfeiffer, K. W. West, and V. Pellegrini, *Science* **332**, 1176 (2011).
- ¹⁹L. Nadvornik, M. Orlita, N. A. Goncharuk, L. Smrcka, V. Novak, V. Jurka, K. Hruska, Z. Vyborny, Z. R. Wasilewski, M. Potemski, and K. Vyborny, *New J. Phys.* **14**, 053002 (2012).
- ²⁰D. Scarabelli, S. Wang, A. Pinczuk, S. J. Wind, Y. Y. Kuznetsova, L. N. Pfeiffer, K. West, G. C. Gardner, M. J. Manfra, and V. Pellegrini, *J. Vac. Sci. Technol. B* **33**, 06FG03 (2015).
- ²¹A. Pinczuk, S. Schmittrink, G. Danan, J. P. Valladares, L. N. Pfeiffer, and K. W. West, *Phys. Rev. Lett.* **63**, 1633 (1989).
- ²²The FWHM of broadening used here (0.2 meV) considers the spectrometer resolution in RILS (0.1 meV) and the variation of diameter of pillars.
- ²³M. L. Sadowski, G. Martinez, M. Potemski, C. Berger, and W. A. de Heer, *Phys. Rev. Lett.* **97**, 266405 (2006).
- ²⁴Z. Jiang, E. A. Henriksen, L. C. Tung, Y. J. Wang, M. E. Schwartz, M. Y. Han, P. Kim, and H. L. Stormer, *Phys. Rev. Lett.* **98**, 197403 (2007).
- ²⁵R. S. Deacon, K. C. Chuang, R. J. Nicholas, K. S. Novoselov, and A. K. Geim, *Phys. Rev. B* **76**, 081406 (2007).
- ²⁶O. P. Sushkov and A. H. Castro Neto, *Phys. Rev. Lett.* **110**, 186601 (2013).
- ²⁷Following Ref. 26, a band gap of 0.4 meV can be opened around Dirac points with lattice constant $L = 40$ nm on nano-patterned p-type GaAs QWs.